

Seasonal variations in the backscatter of RADARSAT-1 images in tropical coastal environments

Sheila Gatinho Teixeira^{1*} , Pedro Walfir Martins e Souza Filho^{2,3} 

Abstract

Understanding the variability in synthetic aperture radar (SAR) backscatter as a function of the phenological variability of vegetation and tropical environmental conditions is still a challenge. Through quantitative and qualitative analyses, this study addresses how both environmental and precipitation conditions, tidal range, and vegetation density affect the backscatter coefficients of coastal environments based on the analysis of four C-band, HH-Polarization, RADARSAT-1 Wide 1 images, in descending orbit, acquired in the wet and dry seasons. The canopy structural variations were analyzed using the enhanced vegetation index (EVI), and correlated with the backscatter values of SAR images, in order to define the predominant backscatter mechanisms, making it possible to distinguish the mangroves from the brackish marshes in the easternmost Amazon coastal plain (Caranguejos Island). The C-band, HH-Polarization RADARSAT-1 backscatter shows the highest correlation with average EVI values in the dry season. The results show that mangroves and brackish marshes can be distinguished in images acquired under low precipitation, especially in the dry season. Variations in the tidal conditions have no effect on the backscatter values of RADARSAT-1 images. We conclude, therefore, that multitemporal RADARSAT-1 images are adequate for monitoring and discriminating wetland environments in a humid tropical climate.

KEYWORDS: synthetic aperture radar; backscatter coefficient; enhanced vegetation index; automatic classification; coastal environments.

INTRODUCTION

For the recognition and mapping of coastal wetland environments using synthetic aperture radar (SAR) images, it is necessary to understand the direct relationships between the parameters of the sensor system: wavelength, (Mougin *et al.* 1999, Lucas *et al.* 2007) polarization (Pope *et al.* 1997, Mougin *et al.* 1999, Lang and Kasischke 2008, Brisco *et al.* 2011, Sang *et al.* 2014), and incidence angle (Wang *et al.* 1995, Singhroy 2002, Kovacs *et al.* 2006, Li *et al.* 2007, Lang *et al.* 2008); as well as characteristics of the targets such as size, geometric shape, density, surface roughness, and dielectric constant (Lewis and Henderson 1998, Tsyganskaya *et al.* 2018). In the C-band SAR, the scattering coefficient Sigma nought (σ°) is mainly influenced by canopy scattering, as greater interaction occurs with the smaller parts of the canopy, such as branches and leaves (Proisy *et al.* 2000, Parmuchi *et al.* 2002, Proisy *et al.* 2002, Townsend 2002, Lang *et al.* 2008). Figure 1 shows the theoretical C-band scattering in a wetland with forest (shrub) vegetation and also in herbaceous vegetation under dry, wet

and flooded soil conditions (Borgeau-Chavez *et al.* 2005, Dabboor and Brisco 2018).

In forests with dense and moist canopies, incident microwave energy is scattered from the canopy layer itself in several directions, reaching the other layers with a smaller amount of energy (Borgeau-Chavez *et al.* 2005). In the case of sparse forests, some microwave radiation penetrates through the tree canopy and interacts with the ground surface, allowing detection of flooding or soil moisture. The transmissivity of the canopy is influenced by the variation in the Leaf Area Index (LAI), which varies over the seasons. In the wet season, when the LAI of the canopy is higher, the canopy transmissivity decreases, as does the amount of energy reaching the forest surface. Consequently, an increase in canopy foliage reduces the ability to detect flooded forests using SAR data (Lang *et al.* 2008). In sparse forests with dry soil, the radiation is scattered in multiple directions from both the tree canopy and the ground surface. When the ground is flooded, most of the energy is scattered in the opposite direction from the smooth surface, then bouncing off the tree trunks back to the sensor (double bounce scattering). In this case, the scattering originating from ground-trunk interactions is often enhanced due to the high dielectric constant of the water and tree trunks (Borgeau-Chavez *et al.* 2005).

In wetlands with herbaceous vegetation on dry soil, multiple scatterings from the vegetation and the ground surface occur, causing a low signal return. With increasing soil moisture, backscattering increases, approaching 11 dB (Dobson and Ulaby 1986) due to an increase in the dielectric constant and possible double bounce scattering due to the interaction of herbaceous

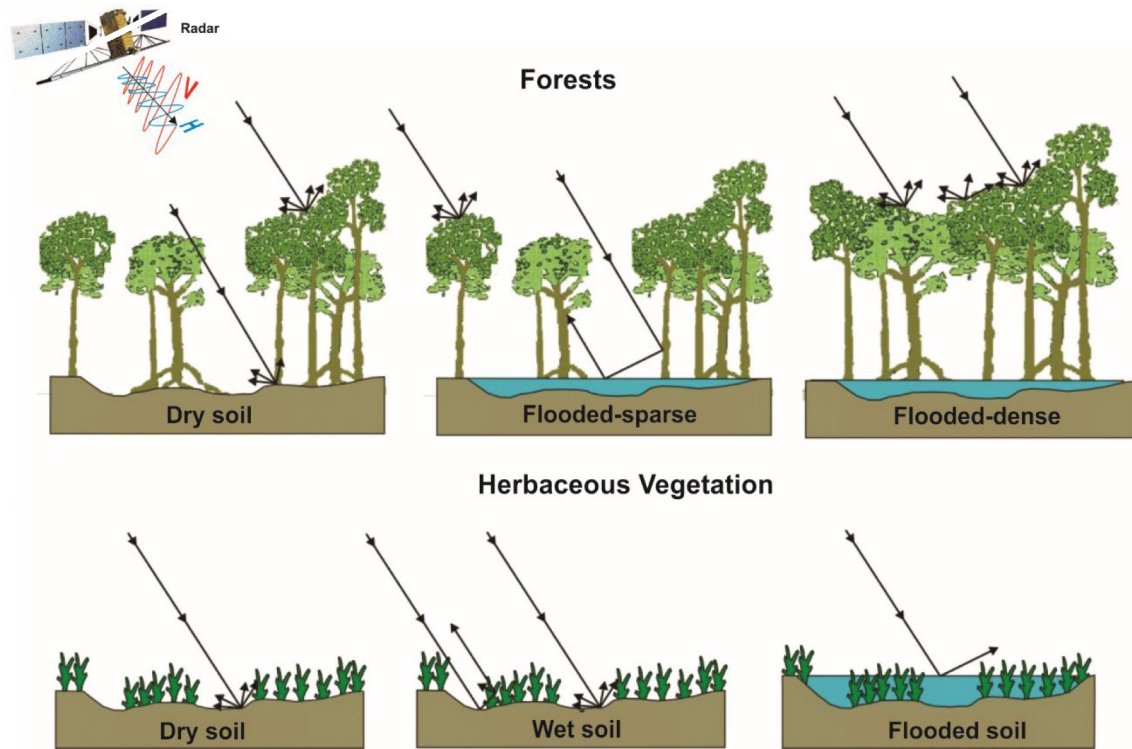
¹Serviço Geológico do Brasil – Belém (PA), Brazil.
E-mail: sheila.teixeira@cprm.gov.br

²Instituto Tecnológico Vale – Belém (PA), Brazil.
E-mail: pedro.martins.souza@itv.org

³Instituto de Geociências, Universidade Federal do Pará – Belém (PA), Brazil. E-mail: walfir@ufpa.br

*Corresponding author.





H: horizontal polarization radar signal; V: vertical polarization radar signal.

Source: adapted from Bourgeau-Chavez *et al.* (2005).

Figure 1. Theoretical model of the C-band scattering of forests and herbaceous vegetation under flooded and nonflooded conditions.

vegetation with the ground (Souza-Filho *et al.* 2011). In the case of a ground surface with flooded vegetation, all incident energy is reflected in the direction opposite that of the sensor, and the backscatter is typically lower than in dry soil (Bourgeau-Chavez *et al.* 2005, Kim *et al.* 2014, Dabboor and Brisco 2018).

Several studies have related radar backscattering with the structural parameters of mangrove vegetation such as basal area (Kovacs *et al.* 2013b), tree height (Simard *et al.* 2006), tree diameter breast height (DBH) (Mougin *et al.* 1999, Kovacs *et al.* 2006, Kovacs *et al.* 2013b), leaf area index (Kovacs *et al.* 2006, Kovacs *et al.* 2013a, Kovacs *et al.* 2013b), stem density (Kovacs *et al.* 2013a); and homogeneous forest canopies to estimate above-ground biomass (AGB) (Van der Sanden 1997, Mougin *et al.* 1999, Proisy *et al.* 2002, Proisy *et al.* 2007, Kovacs *et al.* 2013b, Cougo *et al.* 2015) at various SAR frequencies and polarizations, including C-band and HH-polarization.

In order to map flooded forests, several researchers suggested the use of HH-polarization in comparison to VV-polarization relating to the orientation of the SAR signal for single-polarized data at different wavelengths: C-band (Karszenbaum *et al.* 2000, Townsend 2002, Lang and Kasischke 2008, Sang *et al.* 2014) and considering different frequencies C, L and P-band (Bourgeau-Chavez *et al.* 2001, Proisy *et al.* 2002). In general, HH-polarization penetrates the vegetation canopy better than VV and, when striking the water surface, it reflects better in comparison to VV-polarization. Consequently, the contribution of double-bounce scattering from the trunk-ground interaction is smaller at VV than at HH-polarization (Wang *et al.* 1995, Pierdicca *et al.* 2013).

In the tropical wetlands in the Amazon, the use of C-band SAR imagery has shown satisfactory results in the discrimination

of coastal environments, which are responsible for the enhancement of topographic features, differences in vegetation height, body geometry and moisture content (Souza Filho and Paradella 2001, 2002, Teixeira 2006, Teixeira and Souza-Filho 2009). The boundaries between the mangroves and upland forest in C-band HH-polarization SAR images was well delimited in images acquired in low rainfall for the Golfão Maranhense region (Teixeira and Souza-Filho 2009).

Vegetation indexes obtained from optical images have physical significance (Vygodskaya *et al.* 1989) and several studies have shown the high correlation of EVI — Enhanced Vegetation Index to canopy structural variations, including canopy type, plant physiognomy, and canopy architecture (Wang *et al.* 2013). The EVI is an index designed to enhance the vegetation signal with improved sensitivity in high biomass regions, also improving vegetation monitoring through de-coupling of the canopy background signal and a reduction in atmospheric influences (Justice *et al.* 1998).

Within this context, the goal of the current study is to evaluate the seasonal variations in the backscatter coefficients of RADARSAT-1 images (band C-HH) in coastal wetlands in order to recognize and map mangroves and brackish marshes in relation to the canopy structural variations, through correlation with EVI values in the easternmost Amazon coastal plain.

MATERIALS AND METHODS

Study site

The study site (Fig. 2) is located in the extreme north of the Brazilian state of Maranhão, more precisely, on the Caranguejos

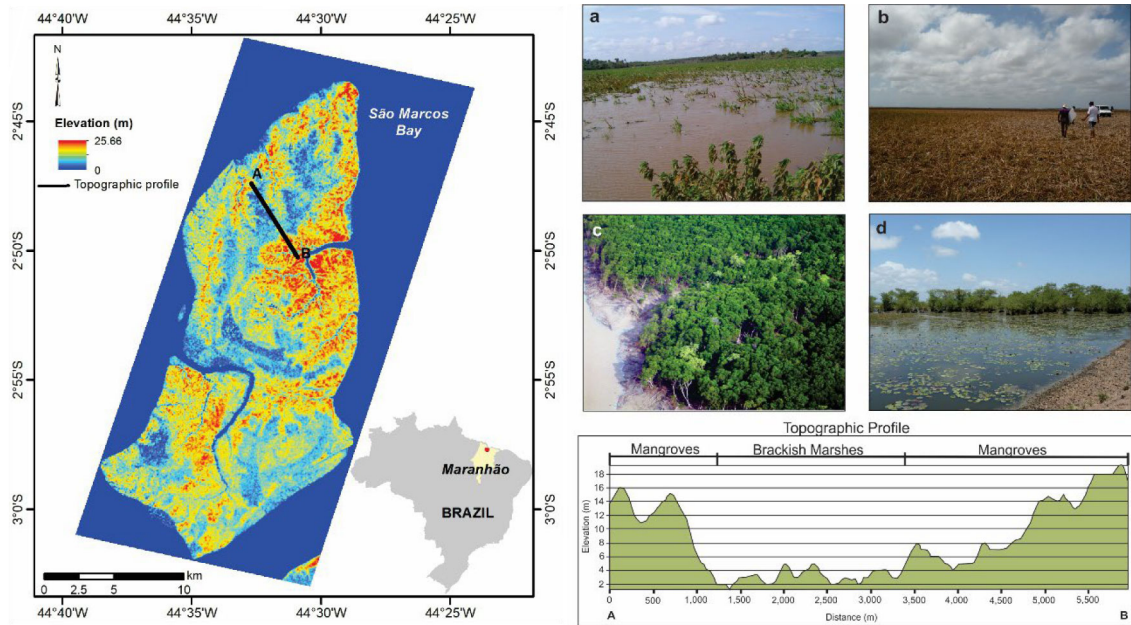


Figure 2. Location of the study site with the digital elevation model (DEM – SRTM – Shuttle Radar Topography Mission) and topographic profile of Caranguejos Island. (A) Brackish marshes in the wet season with shallow water depth; (B) marshes in the dry season; (C) oblique view of *Rhizophora mangle* vegetation; (D) general appearance of the species *Laguncularia racemosa*.

Island in the São Marcos Bay, which is part of the Baixada Maranhense Environmental Protection Area, also the largest mangrove island in Brazil. It has a humid tropical climate characterized by a semidiurnal macrotidal regime, with average tidal range of 4m, a maximum tidal range above 7 m, and maximum tidal currents above 4 m/s (Rebello-Mochel 1997).

Two coastal wetland ecosystems are present in the Caranguejos Island region: mangroves and floodplains. The mangrove forest canopies reach elevations of approximately 25 m, while the floodplains reach approximately 6 m (Fig. 2).

The brackish marshes occur above the high tide of the region, ranging from 4 to 5.7 m and are subject to seasonal flooding (Figs. 2A and 2B), with a water depth of approximately 50 cm during the wet season. The main plant species includes the Cyperaceae family (*Eleocharis mutata*, *Eleocharis caribaea*, *Eleocharis mucronulata* and *Eleocharis interstincta*), grasses (*Paspalum* sp.) and aquatic plants of the genus *Nymphaea* sp. (Rebello-Mochel and Castro 2003).

The mangroves colonize the intertidal zone, which is located along the Maranhão coast at an elevation range between 1.0 and 5.5 m (Rebello-Mochel and Castro 2003). The most common species occurring in the Maranhão mangroves are the *Rhizophora mangle* (Fig. 2C), *Avicennia germinans* (synonymous with *Avicennia nitida*), and *Laguncularia racemosa* (Fig. 2D), especially in areas influenced by salt tides (Rebello-Mochel 1993, 2000).

Remote sensing dataset

Four multitemporal RADARSAT-1 images, with the C-band, Wide-1 mode, and descending orbit, were acquired in the wet and dry seasons under different precipitation conditions and tidal ranges (Tab. 1).

An orthorectified Landsat-4 TM scene (orbit/point 221/062, of 09/13/1992) from the University of Maryland

collection (<http://glcf.umd.edu/data>) was used as the reference image. For the analysis of the EVI, bands 1, 3 and 4 of Landsat-7 ETM+ (orbit/point 221/062, of May 07, 2003) and Landsat-5 TM scenes (orbit/point 221/062, of September 22, 2004) with the lowest cloud cover for the wet and dry seasons, acquired from the digital collection of the Earth Explorer at <https://earthexplorer.usgs.gov>, were used. For the elevation data, Shuttle Radar Topography Mission (SRTM) images from February 2000 (downloaded from <http://www2.jpl.nasa.gov/srtm/>) were used, where the digital elevation model (DEM) was automatically extracted.

Tide level and precipitation data survey

For the evaluation of the tidal conditions (Fig. 3), at the time of acquisition of the SAR images, the tide table data for the Port of Itaqui (São Luís, Maranhão) were analyzed (DHN 2011). The average daily precipitation data (from the São Luís weather station, CPTEC 2006) corresponding to the five days preceding the acquisition of the SAR images, in addition to the average precipitation on the day of acquisition, were used (Fig. 3).

SAR image processing

The RADARSAT-1 images were processed in Geomatica 10.4 using several algorithms (Fig. 4). Initially, headers were read in the CDSAR function, then next step was to read the incidence angles using the Sarinced algorithm. Afterwards, the Sarsigm algorithm was used to correct the brightness values using Equation 1 and Equation 2 was used to calculate the backscatter coefficient values (Raney 1998).

$$\beta^{\circ}(r) = 10 \times \log_{10} \left[\frac{\{DN^2 + A_0\}}{A(r)} \right] \quad (1)$$

$$\sigma^{\circ}(r) = \beta^{\circ}(r) + 10 \times \log_{10} \{ \sin(I(r)) \} \quad (2)$$

Table 1. Characteristics of the RADARSAT-1 images used.

| Platform/Sensor | Beam ode | Polarization | Date of acquisition | Incidence angle (near/far) | Nominal resolution (range x azimuth) (m) | Pixel size (m) | Swath (km) | Season |
|-----------------|-------------|--------------|---------------------|----------------------------------|---|----------------------|---------------|--------|
| RADARSAT-1/SAR | Wide-1 | HH | January 16, 2003 | 20° - 31° | 35.5 x 27 | 12.5 | 165 | Wet |
| RADARSAT-1/SAR | Wide-1 | HH | February 09, 2003 | 20° - 31° | 35.5 x 27 | 12.5 | 165 | Wet |
| RADARSAT-1/SAR | Wide-1 | HH | September 07, 2004 | 20° - 31° | 35.5 x 27 | 12.5 | 165 | Dry |
| RADARSAT-1/SAR | Wide-1 | HH | October 01, 2004 | 20° - 31° | 35.5 x 27 | 12.5 | 165 | Dry |

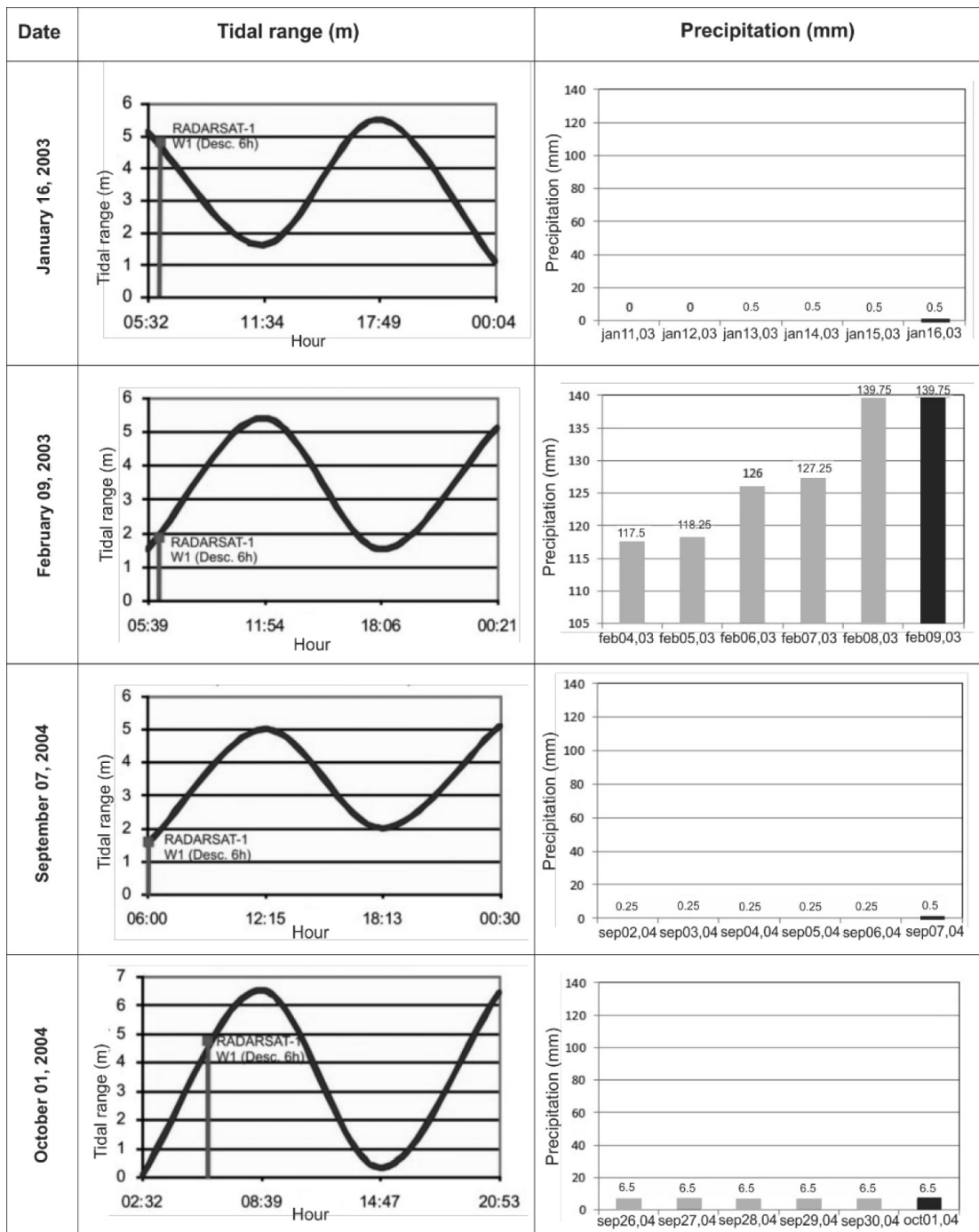


Figure 3. On the left, tidal ranges for the Port of Itaqui (São Luís, Maranhão) on the days when image acquisition occurred (Source: DHN 2011). On the right, precipitation recorded at the São Luís weather station during the 5 days preceding the day of acquisition of the RADARSAT-1 images. The black bar highlights the day of acquisition (Source: CPTEC 2006).

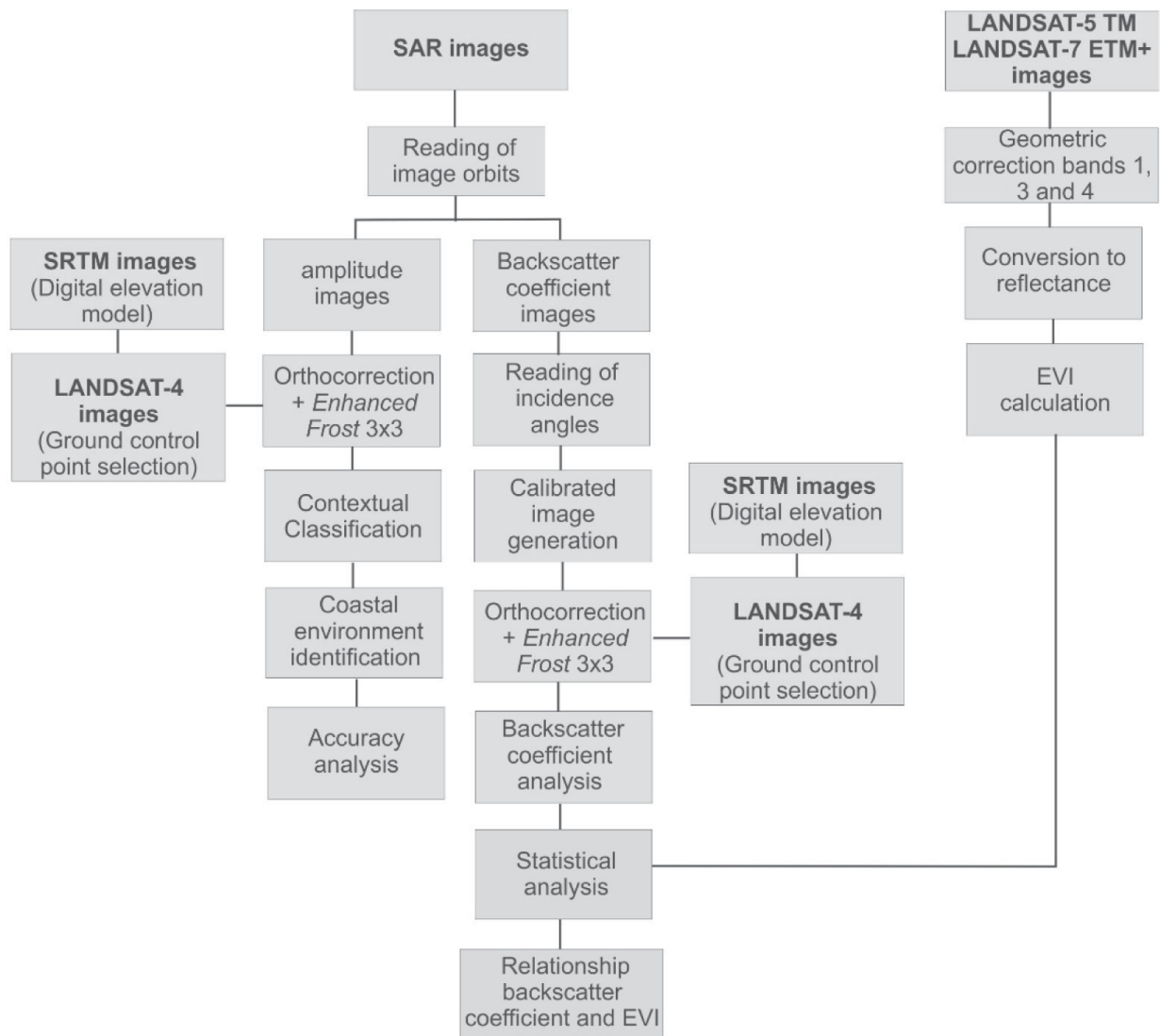


Figure 4. Synthesis of the methodological approach.

Where:

$\beta^\circ(r)$ = image brightness;

$\sigma^\circ(r)$ = backscatter coefficient;

r = image column number (distance in range);

DN2 = numerical value of the pixel;

A0 = scaling;

A(r) = gain offset;

I(r) = incidence angle (varying as a function of distance in range).

Each RADARSAT-1 image (both the amplitude and backscatter coefficient images) was orthorectified in the OrthoEngine package of Geomatica 10.4. The elevation data were extracted from the DEM of the Shuttle Radar Topography Mission-SRTM (Rabus *et al.* 2003), and the control points were obtained from the orthorectified images of Landsat-4 TM. For speckle noise reduction the Enhanced Frost filter was used with a 3x3 window.

For each SAR image, the backscatter coefficient values were collected a total of 50 representative samples, each with a size of 3 x 3 pixels, for each of the classes analyzed (mangroves, brackish marshes and water).

EVI calculation

Initially, the Landsat-5 TM and Landsat-7 ETM+ images were georeferenced using ENVI 5.5. After georeferencing, the gray level values were converted into physical reflectance values in each of the image bands. Atmospheric correction was performed in the FLAASH module with the tropical atmosphere and the rural aerosol models. A single altitude value, 40 m, was used since the Caranguejos Island does not present large altimetric variations. For the visibility parameter, the value of 70 km was applied since a visibility of 40 to 100 is indicated for clear scenes. Lastly, the value of 1.0 was selected as the water column multiplier.

After the transformation from radiance to reflectance, the EVI was calculated according to Equation 3 (Justice *et al.* 1998).

$$EVI = 2.5(\rho_{nir} - \rho_{red}) / (L + \rho_{nir} + C_1\rho_{red} - C_2\rho_{blue}) \quad (3)$$

Where:

EVI = Enhanced vegetation index;

ρ_{nir} = near-infrared band;

ρ_{red} = red band;

ρ_{blue} = blue band;

L = the canopy background correction;
 C_1 and C_2 = the coefficients to correct for aerosol effects.

The coefficients currently used are $L = 1$; $C_1 = 6$ and $C_2 = 7.5$ (Justice *et al.* 1998).

For the extraction of the average EVI values in each of the analyzed classes from the two images, the same polygons were used to extract the backscatter values of the SAR images. Thus, 50 samples of 3 x 3 pixels were collected for each of the classes: mangroves, brackish marshes and water.

Statistical analysis

Statistical analyses were performed using the trial version of the Statistica 10 (StatSoft 2021) software. The average values of the EVI samples and the backscatter coefficients of the SAR images were subjected to exploratory analysis (Kutner *et al.* 2004). Initially, the normality of the distribution of the samples was tested using the Shapiro-Wilk test. Boxplots were constructed to verify the means and dispersion around the mean, in which twice the standard deviation of the sample mean and outliers were adopted. To verify the outliers, the Dixon test was applied to the samples. Subsequently, the similarity between the means of the samples was tested using the Mann-Whitney U test for samples that did not show a normal distribution. The last step was to determine the correlation between the average values of the EVI samples and the backscatter coefficient using the Spearman correlation coefficient (Kutner *et al.* 2004).

Contextual classification

To perform the contextual classification (Gong and Howarth 1992), two 8-bit reduced images were generated from the amplitude images in the Reduce algorithm of Geomatica 10.4. One image for the wet season, using the images from Jan 16, 2003, and Feb 09, 2003 and another for the dry season, using the images from Sep 07, 2004 and Oct 01, 2004.

For the two reduced images, the classification was done using the Context algorithm of PCI 10.4, with the nearest neighbor resampling method and 7x7 window size. Training areas representative of each of the previously determined classes (mangroves, brackish marshes and water) were collected.

The accuracy was assessed by selecting 512 reference points distributed in a stratified and random manner over the study area and comparing them with the reference data collected in the field. In addition, confusion matrices were calculated to evaluate the accuracy of the classification based on the Kappa index, global accuracy and omission and commission error (Congalton 1991).

Figure 4 summarizes the methodological approach used in this study.

RESULTS AND DISCUSSION

Statistical analysis of the backscatter coefficients of the RADARSAT-1 images

The Shapiro-Wilk test confirms the abnormal distribution of the backscatter coefficient samples from the SAR images in all analyzed images at a 5% significance level.

To determine the separability of the environments in the SAR images, first the boxplots are constructed, which facilitates visual analysis based on the mean, dispersion, outliers and extremes (Fig. 5). However, according to the Dixon test, these samples are not confirmed as outliers.

As observed in Figures 5A, 5B, 5C and 5D, the mangroves exhibit the highest mean backscatter coefficient values in all images, followed by the brackish marshes, and the lowest mean values were found in water. Visually, a low dispersion around the mean is observed. For the wet season images, two patterns can be observed. In the Jan 16th, 2003 image, the mangroves are visually separable from the brackish marshes, while in the image from Feb 09th, 2003, some overlap occurs in the dispersions of these two environments, which can make their separation difficult. For the dry season images, the mangroves are separable from the marshes. To determine the similarity of the means of the backscatter values in the water and wetland environments, the data from the samples of the four polarizations were tested using the Mann-Whitney U test as they presented an abnormal distribution (Tab. 2).

The statistical similarity between the mean σ^0 values of the wetlands and the water is not confirmed by the Mann-Whitney U test (Tab. 2). This result confirms that the analyzed classes are separable in the four images, even in the image from Feb 09th, 2003, which shows some overlap of the dispersion of the mean of the marshes and the mangroves (Fig. 5B).

Class separability analysis based on EVI values

The statistical analyses corroborate the recognition and mapping of the water classes of the brackish marshes and mangroves in the two analyzed seasons for EVI. In two analyzed seasons the separation of the brackish marshes and mangroves is difficult, as attested by the Mann-Whitney test.

Through the construction of boxplots, in which the mean, dispersion, outliers and extremes are plotted, a first visual analysis of the separability of the environments in the EVI images can be performed (Fig. 6).

The analysis of Figures 6A and 6B reveals the presence of outliers, which are evaluated by the Dixon test; this test does not confirm their presence. The mean EVI values are similar for the two wetland environments in the two seasons. The visual data analysis shows that there is some overlap in the dispersions of the mean EVI values of the brackish marshes and mangroves in the two seasons, which may lead to some difficulty in distinguishing the environments. The water class is separable from the wetland environments in the two images (Tab. 3).

Analysis of the relationship between the backscatter coefficient and the EVI

The Spearman correlation coefficient (r_s) is used to test the correlation between the σ^0 values and the mean EVI values given the nonparametric nature of the samples. Table 4 shows the correlation coefficient (r_s), the Student's t test probability for n-2 degrees of freedom and the p-values obtained from the correlation test performed between the mean EVI and backscatter values in the wet and dry seasons.

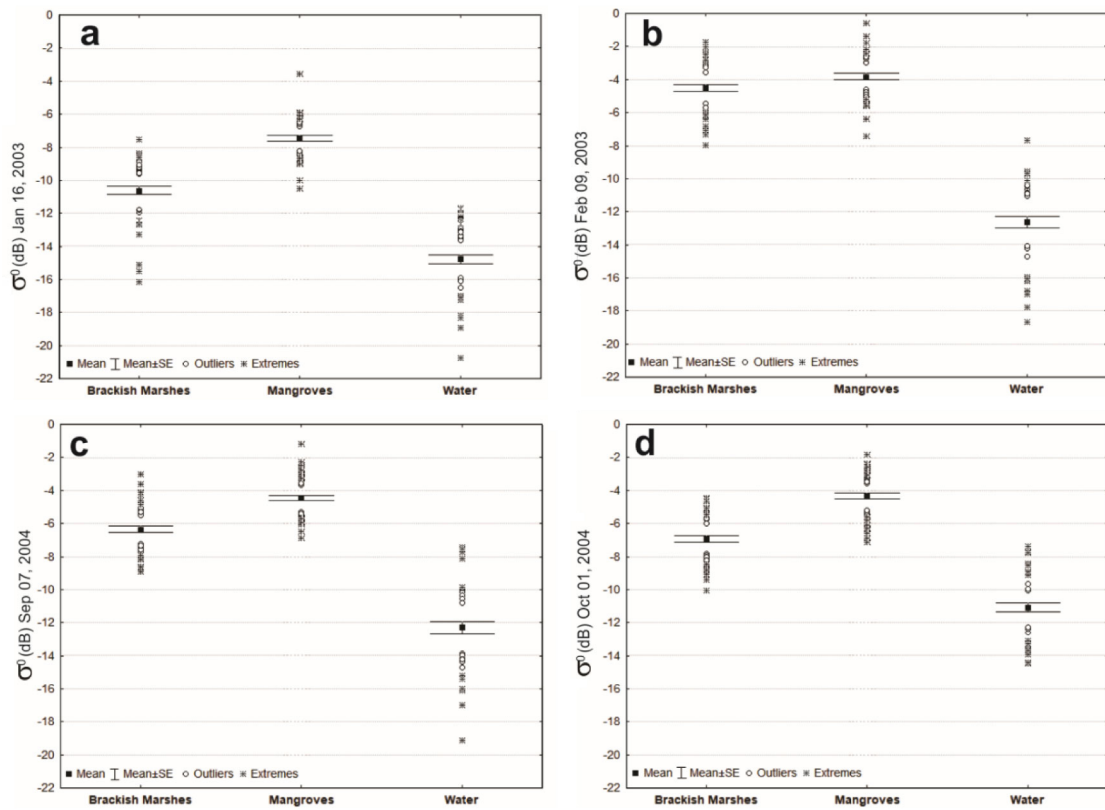


Figure 5. Boxplots of the σ^0 values obtained from the RADARSAT-1 images, for the mangrove environments, brackish marshes and water, in the images acquired on (A) Jan 16, 2003; (B) Feb 09, 2003; (C) Sep 07, 2004; (D) Oct 01, 2004.

Table 2. Mean and standard deviation of σ^0 values extracted from the RADARSAT-1 images and the p-values of the Mann-Whitney U test for comparing the means of σ^0 of the analyzed classes (mangroves, brackish marshes and water) at a 5% significance level.

| | | Water | Brackish Marshes | Mangroves |
|----------------------------|--|--------------|------------------|--------------|
| σ^0 Jan 16, 2003 | Mean | -14.870 | -10.612 | -7.447 |
| | Standard deviation | 1.961 | 1.807 | 1.156 |
| | p-value of U test mean Brackish Marshes | 0.000 | - | 0.000 |
| | p-value of U test mean Mangroves | 0.000 | 0.000 | - |
| σ^0 Feb 09, 2003 | Mean | -12.567 | -4.494 | -3.829 |
| | Standard deviation | 2.393 | 1.441 | 1.348 |
| | p-value of U test mean Brackish Marshes | 0.000 | - | 0.031 |
| | p-value of U test mean Mangroves | 0.000 | 0.031 | - |
| σ^0 Sep 07, 2004 | Mean | -12.336 | -6.356 | -4.457 |
| | Standard deviation | 2.512 | 1.384 | 1.185 |
| | p-value of U test mean Brackish Marshes | 0.000 | - | 0.000 |
| | p-value of U test mean Mangroves | 0.000 | 0.000 | - |
| σ^0 Oct 01, 2004 | Mean | -11.001 | -6.920 | -4.332 |
| | Standard deviation | 1.805 | 1.470 | 1.255 |
| | p-value of U test mean Brackish Marshes | 0.000 | - | 0.000 |
| | p-value of U test mean Mangroves | 0.000 | 0.000 | - |

The results of the Spearman correlation test show that the correlations between the EVI values and the mean backscatter values in all four SAR images are significant at the 5% confidence level, as indicated by the p-value ≈ 0 . The highest correlation values were observed between the mean EVI values with the mean backscatter values in the dry season, showing a

directly proportional relationship. These results indicate that the C-band in the HH polarization is sensitive to variations in vegetation density.

The data presented herein indicates that in the dry season, both mangroves and brackish marshes have high mean EVI values (Tab. 3), are areas related to leaf production rate,

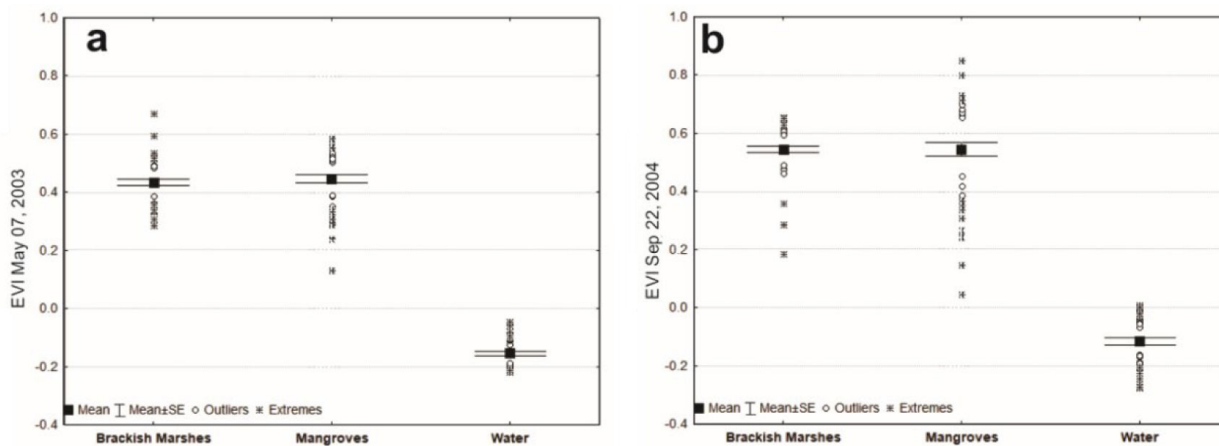


Figure 6. Boxplots of EVI values in the three classes analyzed (mangroves, brackish marshes, and water) in the two season: (A) wet season; (B) dry season.

Table 3. Mean EVI values and standard deviation of the images from May 2003 and September 2004 and p-values of the Mann-Whitney U test for comparing the mean EVI values between the analyzed classes (mangroves, brackish marshes and water), at a 5% significance level.

| | | Water | Brackish marshes | Mangroves |
|-------------------------------|--|--------------|------------------|-----------|
| EVI _{May/2003} | Mean | -0.155 | 0.435 | 0.446 |
| | Standard deviation | 0.050 | 0.075 | 0.095 |
| | p-value of U test mean _{Brackish marshes} | 0.000 | - | 0.150 |
| | p-value of U test mean _{Mangroves} | 0.000 | 0.150 | - |
| EVI _{September/2004} | Mean | -0.116 | 0.544 | 0.545 |
| | Standard deviation | 0.079 | 0.083 | 0.161 |
| | p-value of U test mean _{Brackish Marshes} | 0.000 | - | 0.338 |
| | p-value of U test mean _{Mangroves} | 0.000 | 0.338 | - |

Table 4. Results of the Spearman correlation test between the EVI values and the mean backscatter for the RADARSAT-1 images in the wet and dry seasons.

| | Season | r _s | t(n-2) | p-value |
|-----------------|--------|----------------|--------|---------|
| σ° Jan 16, 2003 | Wet | 0.626 | 9.721 | ≈ 0 |
| σ° Feb 09, 2003 | Wet | 0.644 | 10.211 | ≈ 0 |
| σ° Sep 07, 2004 | Dry | 0.659 | 10.644 | ≈ 0 |
| σ° Oct 01, 2004 | Dry | 0.654 | 10.489 | ≈ 0 |

however this does not correspond immediately to leaf gain in most cases, presenting instead a two- to three-month lag, as presented by Younes *et al.* (2020), in studies of mangrove phenology in Australia, via remote sensing. This is corroborated by Huete *et al.* (2006), who studied the Amazon vegetation phenology through MODIS images and EVI values increased by 25% with sunlight during the dry season. This was attributed to the greater availability of sunlight in the dry season along with uninterrupted root access to deep soil water reserves.

In the wet season, it is believed that the mangrove forest has a less homogeneous and less dense canopy, attested by the lowest mean value EVI (Tab. 3). For the mangrove areas, the *Rhizophora mangle* species, *Laguncularia racemosa* and *Avicennia germinans* produce leaves at different times of the year (Menezes *et al.* 2008), which can influence the mean EVI values and canopy density. The less dense canopy affects microwave radiation interactions since transmissivity tends to

increase, with greater energy interaction in the C-band with the smaller canopy components (Proisy *et al.* 2000, 2002, Lang *et al.* 2008), as shown in Figure 1. Even with higher transmissivity, the energy is not able to reach the water surface under the canopy; thus not having the detection of tidal inundation, which was high at the time of image acquisition on Jan 16, 2003 is not detected. Thus, the backscatter coefficient values for the mangrove forest in this image (mean of approximately -7.4 dB) mainly represent the signal that returned from inside the canopy through volumetric scattering, with the contribution of backscattering from the canopy surface and the interactions of energy with larger branches or trunks (Fig. 7). However, it is believed that much of the incident energy is lost with higher transmissivity. In the image from Feb 09, 2003, it is believed that the high backscatter values, approximately -3.8 dB for the mangrove forest, occur due to an increase in moisture due to the high precipitation recorded for the five days preceding the image acquisition as observed by Kasischke *et al.* (2003), Ali *et al.* (2013) and Wang *et al.* (2013). With an increase in moisture, there was a lower penetration of the incident energy into the canopy and thus a greater signal return as a consequence of volume scattering (Lewis and Henderson 1998).

For the brackish marshes, during the wet season, precipitation and river flooding form shallow water lakes, which allows for greater development of herbaceous plant species (Araujo 2008). Much of the herbaceous vegetation is exposed on the surface of the water layer; thus, the energy recorded by the

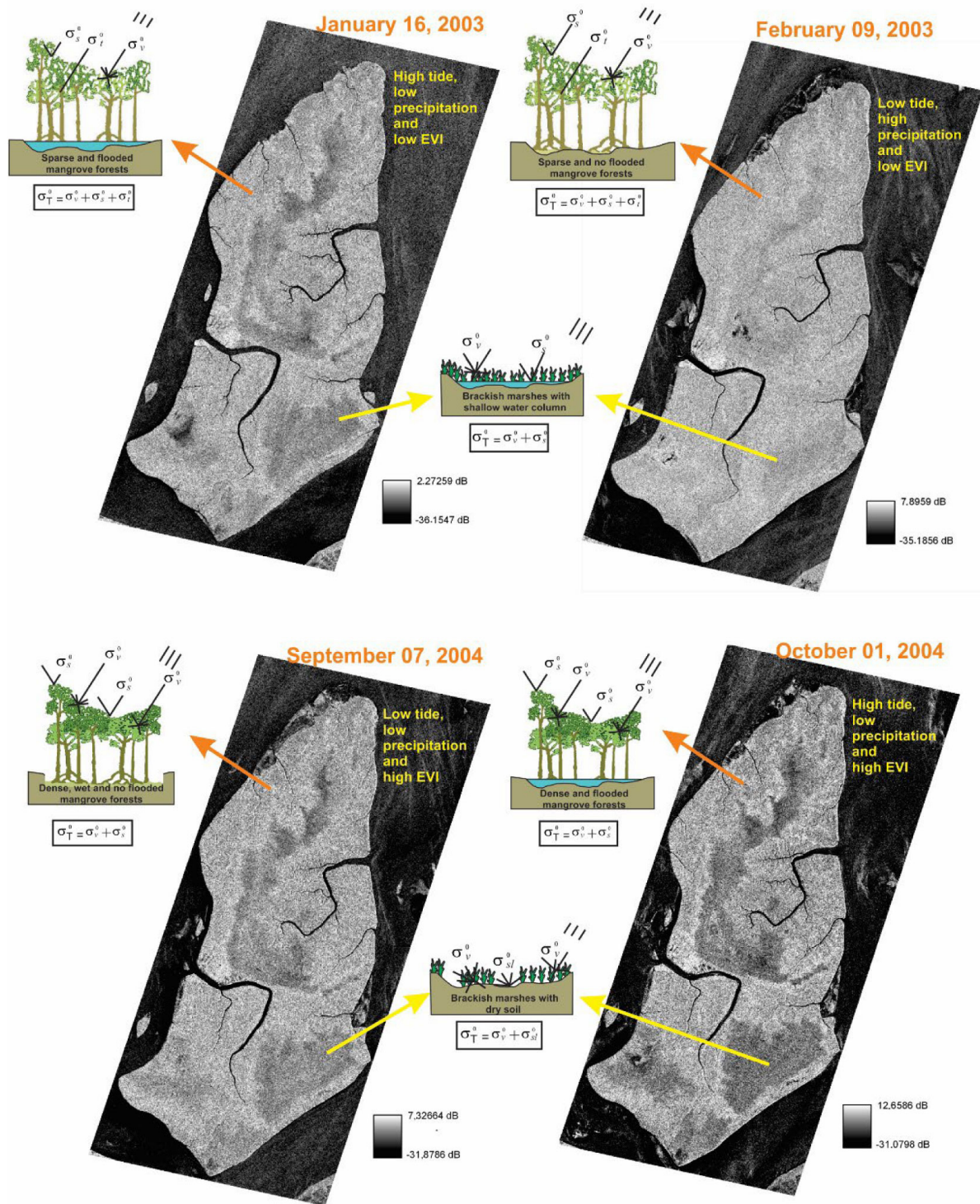


Figure 7. RADARSAT-1 backscatter coefficient images of the wet and dry seasons, where σ_T^0 : total backscatter; σ_s^0 : vegetation surface backscatter; σ_v^0 : volumetric backscatter from inside the vegetation canopy; σ_l^0 : trunk backscatter, σ_{st}^0 : soil surface backscatter and σ_s^0 : specular scattering.

sensor is the energy scattered by the system that functions as a surface of intermediate roughness. The existing vegetation creates a volume scattering and multiple reflections that return to the sensor (Pope *et al.* 1994, 1997, Bourgeau-Chavez *et al.* 2005). However, a part of the incident energy is reflected in the opposite direction from the sensor due to the presence a ground surface with flooded vegetation, and the backscatter is typically lower than in dry soil (Bourgeau-Chavez *et al.* 2005, Kim *et al.* 2014, Dabboor and Brisco 2018), as observed in the image from Jan 16th, 2003 (Fig. 7), where the mean

backscatter values are approximately -10.6 dB. For the image taken in Feb 09th, 2003, the backscatter values of the brackish marshes are higher, approximately -4.4 dB (Tab. 2), which can be explained by the increase in moisture, as previously seen for this image (Wang *et al.* 2013), increasing the intensity of the return of energy back to the sensor (Lewis and Henderson 1998) (Fig. 7).

In the dry season, the mangroves and brackish marshes exhibit high mean EVI values (Tab. 3). These values reflect the increase in leaf production rate (Younes *et al.* 2020), thus it is

believed that the mangrove forest has a more homogeneous and denser canopy. In the two SAR images from the dry season (Sep 07, 2004 and Oct 01, 2004), acquired under low precipitation, the high and low tide conditions do not influence the mean backscatter coefficient values of the mangroves (Tab. 2) since the values, -4.4 and -4.3 dB, respectively, are very close. It is believed that in the dry season, the amount of energy that returns from the mangrove forest back to the sensor is mainly the result of the interaction of scattered radiation in various directions within the canopy (volumetric scattering) with the contribution of backscattering from the canopy surface. The values recorded in the dry season images for the mangrove forest are higher than those recorded in the Jan 16th, 2003 image from the wet season, acquired under low precipitation. As observed by Kovacs *et al.* (2006), who analyzed backscatter values for white mangroves in the Pacific Coast of Mexico using C-band HH- polarization data, captured from a satellite platform (RADARSAT-1 fine beam). It is believed that under denser canopy conditions, a greater amount of incident energy returns to the sensor from the volumetric scattering mechanism, while in canopies with less foliage, a greater amount of incident energy is lost. (Fig. 7).

For the brackish marshes, it is believed that the microwave energy behavior is also the same on the two days of acquisition of the SAR images in the dry season. The high EVI values for the brackish marshes areas may be related to the evaporation of the water layer, which causes the disappearance of aquatic plants, with only grasses and cyperaceous plants remaining, which grow in the shape of tufts. During the summer, these tufts are distant from each other, with the driest leaves exposing

part of the soil. It is believed that with vegetation and exposed soil, the incident microwave energy is scattered in multiple directions from the vegetation and from the ground surface, causing a higher signal return (Fig. 7), when compared to the mean backscatter values recorded in the image from Jan 16th, 2003 (Bourgeau-Chavez *et al.* 2005), thus resulting in backscatter values of approximately -6.0 dB, as seen in Table 2.

Contextual classification of SAR images

As seen in the statistical analysis section, it is possible to separate mangroves, brackish marshes and water in all four images based on the mean backscatter coefficient. Thus, we choose to use contextual classification, based on frequency, as a way to evaluate the separability of the wetland environments in the SAR images in both the wet and dry seasons. Thus, the two images from each season are combined to generate a reduced image for the wet season and another reduced image for the dry season.

Contextual classifications are generated from the reduced images, which are shown in Figures 8A and 8B, for the wet and dry seasons respectively.

By analyzing the confusion matrices presented in Tables 5A and 5B, corresponding to the wet and dry seasons, respectively, we can observe that the brackish marshes exhibit the highest classification error, with commission errors of 35.43% (Tab. 5A) and 19.67% (Tab. 5B). This erroneous classification of pixels, mainly as mangroves, may have been influenced by the Feb 09, 2003 image in the wet season (Fig. 7), in which the responses of the mangroves and brackish marshes were somewhat similar, as shown in Table 2. The difference in

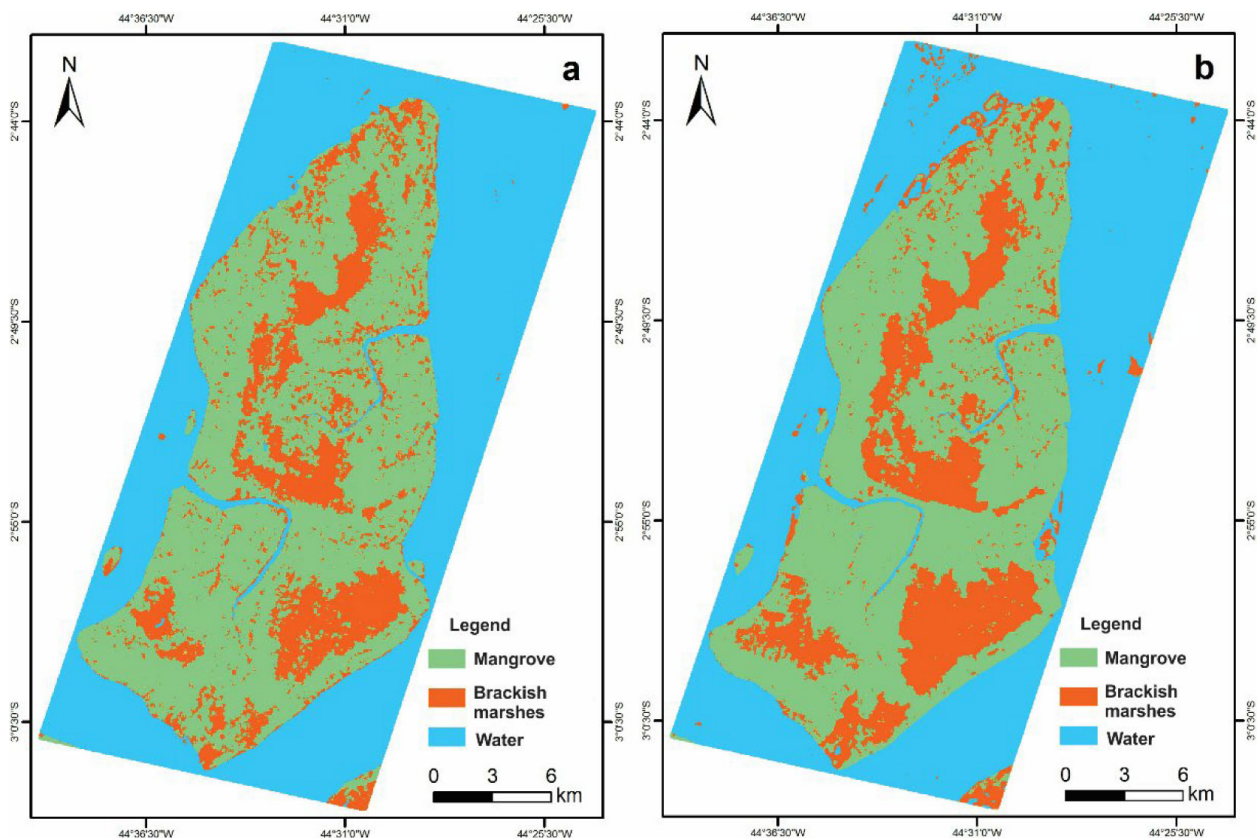


Figure 8. Results of the contextual classifications of the reduced images: (A) wet season and (B) dry season.

Table 5. Confusion matrix generated for the contextual classification of the reduced image: a) wet season and b) dry season.

| <i>Reference Data</i> | | | | | |
|----------------------------------|--------------|-------------------------|------------------|--------------|-----------------------|
| Class | Water | Brackish marshes | Mangroves | \sum_{row} | Commission (%) |
| Water | 190 | 0 | 2 | 192 | 1.04 |
| Brackish marshes | 7 | 82 | 38 | 127 | 35.43 |
| Mangroves | 4 | 35 | 154 | 193 | 20.21 |
| \sum_{column} | 201 | 117 | 194 | 512 | |
| Omission (%) | 5.47 | 29.91 | 20.61 | | |
| Kappa index = 0.743 | | | | | |
| Overall accuracy = 83.20% | | | | | |
| <i>Reference Data</i> | | | | | |
| Class | Water | Brackish marshes | Mangroves | \sum_{row} | Commission (%) |
| Water | 185 | 0 | 3 | 188 | 1.59 |
| Brackish marshes | 6 | 98 | 18 | 122 | 19.67 |
| Mangroves | 2 | 28 | 171 | 201 | 14.92 |
| \sum_{column} | 194 | 126 | 192 | 512 | |
| Omission (%) | 4.64 | 22.22 | 10.94 | | |
| Kappa index = 0.827 | | | | | |
| Overall accuracy = 88.67% | | | | | |

the mean backscatter between these two environments is less than 1 dB, which is caused by the increase in moisture, which generally increases the backscattering of the image, as previously seen. For the dry season, the confusion may be caused by the classification of dense mangrove areas as brackish marshes areas.

An evaluation of the overall accuracy index indicates that the contextual classification of the dry season image is slightly better than the classification of the reduced wet season image. The tables show that the contextual classification of the dry season presents the highest kappa index (82.7%), thus indicating excellent performance according to the classification of Cohen (1960).

CONCLUSION

The qualitative and quantitative analyses of the RADARSAT-1 images and of the mean σ° values of the mangrove forests and brackish marshes showed that these environments are separable in C-band SAR images, especially when the images acquired in areas under low precipitation conditions. When there is moisture in the system, the separation between these environments tends to decrease due to increased backscatter. The mean backscatter values of the mangroves were always higher than the mean values of the brackish marshes, corroborating the idea that the amount of energy that returns back to the sensor from the volumetric scattering that occurs in the canopy of mangrove forests is greater than the energy that returns from the diffuse scattering of the brackish marshes.

The C-band HH-polarization backscatter coefficients were correlated to spectral vegetation indexes — EVI, and the highest correlation values were observed between values in dry season, corroborating the idea that the C-band in the HH-polarization is sensitive to variations in vegetation density.

The contextual classification method was considered efficient in the mapping of wetlands in both seasons since very good classifications were presented for the wet season and excellent classifications were presented for the dry season. The multitemporal RADARSAT-1 images were adequate for the monitoring and discrimination of wetlands in humid tropical climates and allowed for the evaluation of the influence of the interaction of environmental conditions on the backscatter of microwave radiation from coastal wetlands.

This study proved that the HH-polarization was efficient for distinguishing the contact between mangroves and the brackish marshes, corroborating the idea that HH-polarization penetrates the vegetation canopy even with a difference in structure.

In addition, other polarizations can be used and compared in future research and, furthermore, the results found can serve as a reference for similar studies using Sentinel images.

ACKNOWLEDGMENTS

The authors are grateful to Petrobras for financial support through the PIATAM Mar project for fieldwork support. S.G.T. would like to thank CNPq for a Ph.D. scholarship, while P.W.M.S.F would like to thank CNPq for the research grant received for this research.

ARTICLE INFORMATION

Manuscript ID: 20210077. Received on: 21 DEC 2020. Approved on: 07 FEB 2022.

How to cite this article: Teixeira S.G., Souza Filho P.W.M. Seasonal variations in the backscatter of RADARSAT-1 images in tropical coastal environments. *Brazilian Journal of Geology*, 52(1):e20210062, 2022. <https://doi.org/10.1590/2317-488920220210077>.

S.T. wrote the first draft of the manuscript and prepared all figures; P.S.F. improved the manuscript through corrections and suggestions about backscatter values of RADARSAT-1 images.

Competing interests: The authors declare no competing interests.

REFERENCES

- Ali I., Schuster C., Zebisch M., Forster M., Kleinschmit B., Notarnicola C. 2013. First results of monitoring nature conservation sites in alpine region by using very high resolution (VHR) X-band SAR data. *IEEE Journal of Selected Topics in Applied Earth Observations and Remote Sensing*, **6**(5):2265-2274. <https://doi.org/10.1109/JSTARS.2013.2241735>
- Araujo N.A. 2008. *Relações ecológicas entre a fauna ictiológica e a vegetação ciliar da região lacustre do Baixo Pindaré na baixada maranhense e suas implicações na sustentabilidade da pesca regional*. Dissertação de Mestrado, Centro de Ciências Biológicas e da Saúde, Universidade Federal do Maranhão, São Luis, 122 p.
- Bourgeau-Chavez L.L., Kasischke E.S., Brunzell S.M., Mudd J.P., Smith K.B., Frick A.L. 2001. Analysis of Space-Borne SAR Data for Wetland Mapping in Virginia Riparian Ecosystems. *International Journal of Remote Sensing*, **22**(18):3665-3687. <https://doi.org/10.1080/01431160010029174>
- Bourgeau-Chavez L.L., Smith K.B., Brunzell S.M., Kasischke E.S., Romanowicz E.A., Richardson C.J. 2005. Remote sensing of regional inundation patterns and hydroperiod in the greater Everglades using synthetic aperture radar. *Wetlands*, **25**:176-191. [https://doi.org/10.1672/0277-5212\(2005\)025\[0176:RMORIP\]2.0.CO;2](https://doi.org/10.1672/0277-5212(2005)025[0176:RMORIP]2.0.CO;2)
- Brisco B., Kapfer M., Hirose T., Tedford B., Liu J. 2011. Evaluation of C-Band Polarization Diversity and Polarimetry for Wetland Mapping. *Canadian Journal of Remote Sensing*, **37**(1):82-92. <https://doi.org/10.5589/m11-017>
- Centro de Previsão de Tempo e Estudos Climáticos (CPTEC). 2006. Observações e Instrumentação – Dados Automáticos – Plataformas de Coleta de Dados. Available in: <http://sinda.crn.inpe.br/PCD/SITE/novo/site/index.php>. Accessed on: July 15, 2006.
- Cohen J.A. 1960. Coefficient of agreement for nominal scales. *Educational and Psychological Measurement*, **20**(1):37-46. <https://doi.org/10.1177%2F001316446002000104>
- Congalton R. 1991. A review of assessing the accuracy of classification or remotely sensed data. *Remote Sensing of Environment*, **37**(1):35-45. [https://doi.org/10.1016/0034-4257\(91\)90048-B](https://doi.org/10.1016/0034-4257(91)90048-B)
- Cougo M.F., Souza-Filho P.W.M., Silva A.Q., Fernandes M.E.B., Santos J.R., Abreu M.R.S., Nascimento W.R., Simard M. 2015. Radarsat-2 Backscattering for the Modeling of Biophysical Parameters of Regenerating Mangrove Forests. *Remote Sensing*, **7**(12):17097-17112. <https://doi.org/10.3390/rs71215873>
- Daboor M., Brisco B. 2018. Wetland monitoring and mapping using synthetic aperture radar. In: Gokce D. (ed.). *Wetlands management: assessing risk and sustainable solutions*. London: Intechopen, p. 61-86.
- Diretoria de Hidrografia e Navegação (DHN). 2011. *Previsões de Maré – Terminal da ALUMAR Estação do Maranhão*. Available in: <https://www.marinha.mil.br/chm/tabuas-de-mare>. Accessed on: June 5, 2011.
- Dobson M.C., Ulaby F.T. 1986. Active microwave soil moisture research. *IEEE Transactions on Geoscience and Remote Sensing*, **24**(1):23-36. <https://doi.org/10.1109/TGRS.1986.289585>
- Gong P., Howarth P.J. 1992. Frequency-based contextual classification and gray-level vector reduction for land-use identification. *Photogrammetric Engineering & Remote Sensing*, **58**(4):423-437.
- Huete A.R., Didan K., Shimabukuro Y.E., Ratana P., Saleska S.R., Hutyrá L.R., Yang W., Nemani R.R., Myneni R. 2006. Amazon rainforests green-up with sunlight in dry season. *Geophysical Research Letters*, **33**(6):1-4. <https://doi.org/10.1029/2005GL025583>
- Justice C.O., Vermote E., Townshend J.R.G., Defries R., Roy D.P., Hall D.K., Salomonson V.V., Privette J.L., Riggs G., Strahler A., Lucht W., Myneni R.B., Knyazikhin Y., Running S.W., Nemani R.R., Zhengming W., Huete A.R., Van Leeuwen W., Wolfe R.E., Giglio L., Muller J., Lewis P., Barnsley M.J. 1998. The Moderate Resolution Imaging Spectroradiometer (MODIS): land remote sensing for global change research. *IEEE Transactions on Geoscience and Remote Sensing*, **36**(4):1228-1249. <https://doi.org/10.1109/36.701075>
- Karszenbaum H., Kandus P., Martinez J.M., Le Toan T., Tiffenberg J., Parmuchi G. 2000. ERS-2, Radarsat SAR Backscattering Characteristics of the Parana River Delta Wetland, Argentina. *Special Publication*, SP-461.
- Kasischke E.S., Smith K.B., Bourgeau-Chavez L.L., Romanowicz E.A., Brunzell S.M., Richardson C.J. 2003. Effects of seasonal hydrologic patterns in south Florida wetlands on radar backscatter measured from ERS-2 SAR imagery. *Remote Sensing of Environment*, **88**(4):423-441. <https://doi.org/10.1016%2Fj.rse.2003.08.016>
- Kim J.-W., Lu Z., Jones J.W., Shum C.K., Lee H., Jia Y. 2014. Monitoring Everglades freshwater marsh water level using L-band synthetic aperture radar backscatter. *Remote Sensing of Environment*, **150**:66-81. <https://doi.org/10.1016/j.rse.2014.03.031>
- Kovacs J.M., Jiao X., Flores-de-Santiago F., Zhang C., Flores-Verdugo F. 2013a. Assessing relationships between Radarsat-2 C-band and structural parameters of a degraded mangrove forest. *International Journal of Remote Sensing*, **34**(20):7002-7019. <https://doi.org/10.1080/01431161.2013.813090>
- Kovacs J.M., Lu X.X., Flores-Verdugo F., Zhang C., Flores de Santiago F., Jiao X. 2013b. Applications of ALOS PALSAR for monitoring biophysical parameters of a degraded black mangrove (*Avicennia germinans*) forest. *ISPRS Journal of Photogrammetry and Remote Sensing*, **82**:102-111. <https://doi.org/10.1016/j.isprsjprs.2013.05.004>
- Kovacs J.M., Vandenberg C.V., Flores-Verdugo F. 2006. Assessing fine beam RADARSAT-1 backscatter from a white mangrove (*Laguncularia racemosa* (Gaertner)) canopy. *Wetlands Ecology and Management*, **14**:401-408. <https://doi.org/10.1007/s11273-005-6237-x>
- Kutner M.N., Nachtsheim C.J., Neter J., Li W. 2004. *Applied linear statistical models*. 5. ed. Boston: WCB/McGraw-Hill, 1396 p.
- Lang M.W., Kasischke E.S. 2008. Using C-band synthetic aperture radar data to monitor forested wetland hydrology in Maryland's coastal plain, USA. *IEEE Transactions on Geoscience and Remote Sensing*, **46**(2):535-546. <https://doi.org/10.1109/TGRS.2007.909950>
- Lang M.W., Townsend P.A., Kasischke E.S. 2008. Influence of incidence angle on detecting flooded forests using C-HH synthetic aperture radar data. *Remote Sensing of Environment*, **112**(10):3898-3907. <https://doi.org/10.1016/j.rse.2008.06.013>
- Lewis A.J., Henderson F.M. 1998. Radar fundamentals: the geoscience perspective. In: Henderson F.M., Lewis A.J. (eds.). *Principles & applications of imaging radar: manual of remote sensing*. 3. ed. New York, John Wiley, p. 131-181.
- Li J., Chen W., Touzi R. 2007. Optimum RADARSAT-1 configurations for wetlands discrimination: a case study of the Mer Bleue peat bog. *Canadian Journal Remote Sensing*, **33**(Suppl. 1):S46-S55. <https://doi.org/10.5589/m07-046>
- Lucas R.M., Mitchell A.L., Rosenqvist A., Proisy C., Melius A., Ticehurst C. 2007. The potential of L-band SAR for quantifying mangrove characteristics and change: case studies from the tropics. *Aquatic Conservation: Marine and Freshwater Ecosystems*, **17**(3):245-264. <https://doi.org/10.1002/aqc.833>
- Menezes M.P.M., Berger U., Mehig U. 2008. Mangrove vegetation in Amazonia: a review of studies from the coast of Pará and Maranhão States, north Brazil. *Acta Amazonica*, **38**(3):403-420. <https://doi.org/10.1590/S0044-59672008000300004>

- Mougin E., Proisy C., Marty G., Fromard F., Puig H., Betoulle L., Rudant J.P. 1999. Multifrequency and multipolarization radar backscattering from mangrove forests. *IEEE Transactions on Geoscience and Remote Sensing*, **37**(1):94-102. <https://doi.org/10.1109/36.739128>
- Parmuchi M.G., Karszenbaum H., Kandus P. 2002. Mapping wetlands using multi-temporal RADARSAT-1 data and decision-based classifier. *Canadian Journal Remote Sensing*, **28**(2):175-186. <https://doi.org/10.5589/m02-014>
- Pierdicca N., Pulvirenti L., Chini M., Guerriero L., Candela L. 2013. Observing floods from space: experience gained from COSMO-SkyMed observations. *Acta Astronautica*, **84**:122-133. <https://doi.org/10.1016/j.actastro.2012.10.034>
- Pope K.O., Rejmankova E., Paris J.F., Woodfruff R. 1997. Detecting seasonal flooding cycles in marshes of the Yucatan Peninsula with SIR-C polarimetric radar imagery. *Remote Sensing of Environment*, **59**:157-166.
- Pope K.O., Rey-Benayas J.M., Paris J.F. 1994. Radar remote sensing of forest and wetland ecosystems in the Central American tropics. *Remote Sensing of Environment*, **48**(2):205-219. [https://doi.org/10.1016/0034-4257\(94\)90142-2](https://doi.org/10.1016/0034-4257(94)90142-2)
- Proisy C., Couteron P., Fromard, F. 2007. Predicting and mapping mangrove biomass from canopy grain analysis using Fourier-based textural ordination of IKONOS images. *Remote Sensing of Environment*, **109**(3):379-392. <https://doi.org/10.1016/j.rse.2007.01.009>
- Proisy C., Mougin E., Fromard F., Karam M.A. 2000. Interpretation of polarimetric radar signatures of mangrove forests. *Remote Sensing of Environment*, **71**(1):56-66. [https://doi.org/10.1016/S0034-4257\(99\)00064-4](https://doi.org/10.1016/S0034-4257(99)00064-4)
- Proisy C., Mougin E., Fromard F., Trichon V., Karam M.A. 2002. On the influence of canopy structure on the radar backscattering of mangrove forests. *International Journal of Remote Sensing*, **23**(20):4197-4210. <https://doi.org/10.1080/01431160110107725>
- Rabus B., Eineder M., Roth A., Bamler R. 2003. The shuttle radar topography mission – a new class of digital elevation models acquired by spaceborne radar. *ISPRS Journal of Photogrammetry and Remote Sensing*, **57**(4):241-262. [https://doi.org/10.1016/S0924-2716\(02\)00124-7](https://doi.org/10.1016/S0924-2716(02)00124-7)
- Raney K. 1998. Radar fundamentals: technical perspective. In: Henderson F.M., Lewis A.J. (eds.). *Principles & applications of imaging radar: manual of remote sensing*. 3. ed. New York, John Wiley, p. 8-130.
- Rebello-Mochel F. 1993. Mangroves of Maranhão State, North Brazil. In: Workshop on Conservation and Sustainable Utilization of Mangrove Forests in Latin America and Africa Regions, 1., 1993. *Proceedings...* p. 14.
- Rebello-Mochel F. 1997. Mangroves on São Luís Island, Maranhão, Brazil. In: Kjerfve B., Lacerda L.D., Diop E.H.S. (eds). *Mangrove ecosystem studies in Latin America and Africa*. Paris: UNESCO, p. 145-154.
- Rebello-Mochel F. 2000. Structural variability of mangrove forest influenced by sewerage in Turiaçu Bay, Amazonian coast of Maranhão, Brazil. In: *Mangrove 2000 Conference*, Recife, Brazil. *Proceedings...*
- Rebello-Mochel F., Castro A.C.L. 2003. *Zonamento costeiro do estado do Maranhão*. São Luís, Laboratório de Hidrobiologia, Universidade Federal do Maranhão, 243 p.
- Sang H., Zhang J., Lin H., Zhai L. 2014. Multi-Polarization ASAR Backscattering from Herbaceous Wetlands in Poyang Lake Region, China. *Remote Sensing*, **6**(5):4621-4646. <https://doi.org/10.3390/rs6054621>
- Simard M., Zhang K., Rivera-Monroy V.H., Ross M.S., Ruiz P.L., Castañeda-Moya E., Twilley R.R., Rodrigues E. 2006. Mapping height and biomass of mangrove forests in everglades National Park with SRTM elevation data. *Photogrammetric Engineering and Remote Sensing*, **72**(3):299-311. <https://doi.org/10.14358/PERS.72.3.299>
- Singhroy V. 2002. SAR incidence angles for mapping areas affected by geological hazards, tropical case studies. *Asian Journal of Geoinformatics*, **2**(3):53-57. <https://doi.org/10.4095/219970>
- Souza Filho P.W.M., Paradella W.R. 2001. Estudos da geomorfologia de ambientes costeiros tropicais úmidos a partir de imagens de sensores remotos. *Revista Pesquisas*, **28**(2):359-368. <https://doi.org/10.22456/1807-9806.20310>
- Souza Filho P.W.M., Paradella W.R. 2002. Recognition of the main geobotanical features in the Bragança mangrove coast (Brazilian Amazon Region) from Landsat TM e RADARSAT-1 data. *Wetlands Ecology and Management*, **10**(2):121-130. <https://doi.org/10.1023/A:1016527528919>
- Souza-Filho P.W.M., Paradella W.R., Rodrigues S.W.P., Costa F.R., Mura J.C., Gonçalves F.D. 2011. Discrimination of coastal wetland environments in the Amazon region based on multi-polarized L-band airborne Synthetic Aperture Radar imagery. *Estuarine, Coastal and Shelf Science*, **95**(1):88-98. <https://doi.org/10.1016/j.ecss.2011.08.011>
- StatSoft. 2021. Statistica, Version 10. Available in: <https://www.statistica.com/en/>. Accessed on: Sept 18, 2021.
- Teixeira S.G. 2006. *Análise de imagens de sensores remotos orbitais para mapeamento de ambientes costeiros tropicais e de índices de sensibilidade ambiental ao derramamento de óleo no Golfo Maranhense*. Dissertação de Mestrado, Centro de Geociências, Universidade Federal do Pará, Belém, 171 p.
- Teixeira S.G., Souza-Filho P.W.M. 2009. Mapeamento de ambientes costeiros tropicais (Golfo Maranhense, Brasil) utilizando imagens de sensores remotos orbitais. *Revista Brasileira de Geofísica*, **27**(Suppl. 1):69-82. <https://doi.org/10.1590/S0102-261X2009000500006>
- Townsend P.A. 2002. Relationships between forest structure and the detection of flood inundation in forested wetlands using C-Band SAR. *International Journal of Remote Sensing*, **23**(3):443-460. <https://doi.org/10.1080/01431160010014738>
- Tsyganskaya V., Martinis S., Marzahn P., Ludwig R. 2018. SAR-based detection of flooded vegetation – a review of characteristics and approaches. *International Journal of Remote Sensing*, **39**(8):2255-2293. <https://doi.org/10.1080/01431161.2017.1420938>
- Van Der Sanden J.J. 1997. *Radar remote sensing to support tropical forest management*. Thesis (Doctorate), Wageningen Agricultural University, Wageningen.
- Vygodskaya N.N., Gorshkova I., Fadeyeva Ye V. 1989. Theoretical estimates of sensitivity in some vegetation indices to variation in the canopy condition. *International Journal of Remote Sensing*, **10**(12):1857-1872. <https://doi.org/10.1080/01431168908904016>
- Wang X., Ge L., Li X. 2013. Pasture Monitoring Using SAR with COSMO-SkyMed, ENVISAT ASAR, and ALOS PALSAR in Otway, Australia. *Remote Sensing*, **5**(7):3611-3636. <https://doi.org/10.3390/rs5073611>
- Wang Y., Hess L.L., Foloso S., Melack J.M. 1995. Understanding the Radar Backscattering from flooded and nonflooded Amazonian forests: Results from canopy backscatter modeling. *Remote Sensing of Environment*, **54**(3):324-332. [https://doi.org/10.1016/0034-4257\(95\)00140-9](https://doi.org/10.1016/0034-4257(95)00140-9)
- Younes N., Northfield T.D., Joyce K.E., Maier S.W., Duke N.C., Lymburner L. 2020. A novel approach to modelling mangrove phenology from satellite images: a case study from Northern Australia. *Remote Sensing*, **12**(24):4008. <https://doi.org/10.3390/rs12244008>